Ni–Nb-Based Mixed Oxides Precursors for the Dry Reforming of Methane

Topics in Catalysis

ISSN 1022-5528
Volume 54
Combined 1-4

Top Catal (2011) 54:170-178
DOI 10.1007/
s11244-011-9636-7

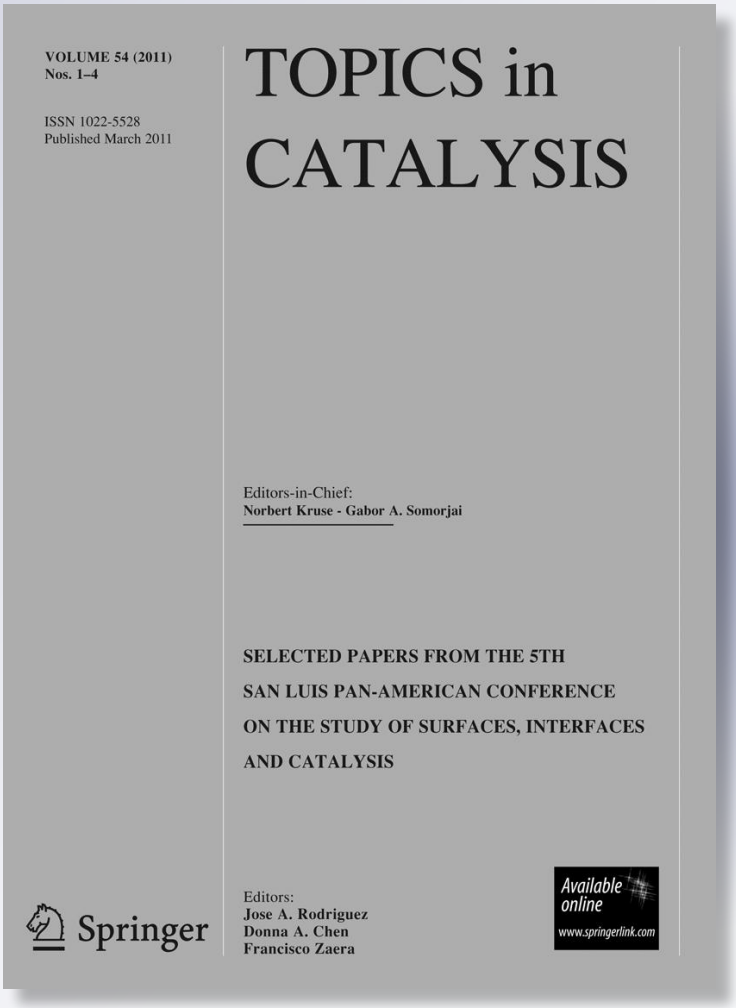

Springer

Top Catal (2011) 54:170–178
DOI 10.1007/s11244-011-9636-7

ORIGINAL PAPER

Ni–Nb-Based Mixed Oxides Precursors for the Dry Reforming of Methane

Juan Alvarez · Gustavo Valderrama · Eglé Pietri · María Josefina Pérez-Zurita · Caribay Urbina de Navarro · Eduardo Falabella Sousa-Aguiar · Mireya R. Goldwasser

Published online: 21 January 2011

Abstract Perovskite-related mixed-oxides based on La Ni Nb and La Sr Ni Nb were synthesized by the auto combustion method to use as precursors materials for the catalytic reforming of methane at 700 °C, atmospheric pressure, CH_4:CO_2 = 1:1. $LaNiO_3$ and $LaNbO_4$ were used as reference. XRD analysis show that the synthesis method produce a new series of precursor family formed by a mixture of oxides where Ni crystallized as part of a perovskite and Ruddlesden–Popper structure while Nb formed lanthanum orthoniobate $LaNbO_4$, a scheelite-type structure alternating with oxide layers, with phase distribution depending on niobium content. For Nb ($x \leq 0.3$) Ni crystallizes as $LaNiO_3$ perovskite-type oxide while for Nb ($x \geq 0.7$) it forms mainly the orthoniobate phase $LaNbO_4$ a scheelite-type structure. At higher calcined temperatures (~1100 °C) $La_2Ni_{0.8}Nb_{0.2}O_4$ was formed with a Ruddlesden–Popper structure consisting of three perovskite type layers along the *c*-axis alternating with a layer of the rock salt type phase. TEM analysis showed the presence of cubic particles with sizes varying between 5 and 60 nm depending on the extent of substitution of Ni by Nb. Reduction of the perovskite-related precursor oxides produced a series of Ni^0/La_2O_3–NbOx oxides with high metallic dispersion which favors the activity and stability of the catalysts. Introduction of doping quantities of Sr into $LaNi_{0.8}Nb_{0.2}O_{3\pm\lambda}$ structure produced a mixture of oxides with Sr dissolved in the lanthanum orthoniobate $LaNbO_4$ scheelite-type structure due to the similarity of ionic radii of La and Sr. Under the reaction conditions conversions near the thermodynamic equilibrium were attained which remains for long periods of time assessing the stability of the synthesized catalysts.

Keywords Ni–Nb-mixed oxides · Dry methane reforming · Perovskites-related structures · Ruddlesden–Popper structure · Scheelite structure

1 Introduction

A long way has passed since natural gas was considered as a sub-product of crude exploitation. Due to its abundance, cleanness and diversity of applications, it is estimated that for the year 2025 it will be the most used fuel globally [1]. Great diversity of applications has emerged and renews interest is focused on the development of new technologies to liquid fuels to meet the more demanding environmental regulations since increasingly stringent legislations necessitate a new approach to the control of vehicles emissions [2, 3].

Valorization of natural gas could be carried out by its transformation to syngas, a mixture of hydrogen and carbon monoxide which is a feedstock to more valuable

J. Alvarez · G. Valderrama · E. Pietri · M. J. Pérez-Zurita · M. R. Goldwasser (✉)
Centro de Catálisis, Petróleo y Petroquímica, Escuela de Química, Caracas, Venezuela
e-mail: mireya.goldwasser@ciens.ucv.ve

C. U. de Navarro
Centro de Microscopía Electrónica, Facultad de Ciencias, Universidad Central de Venezuela, Apartado 40600, Los Chaguaramos, Caracas 1040, Venezuela

E. F. Sousa-Aguiar
CENPES/Petrobras, Cidade Universitaria, Ilha do Fundacao, Quadra 7, Rio de Janeiro, RJ, Brazil

E. F. Sousa-Aguiar
Petrobras, Cenpes, Avenida Rio Branco n 1 - 20 andar—Centro, CEP 20090 907, Rio de Janeiro, RJ, Brazil

products, by means of methane reforming, major component of natural gas, through several reactions such as steam reforming, partial oxidation, auto-thermal reforming and combine and dry reforming [5–8]. The dry reforming has been proposed as an important reaction especially for its environmental quality, due to the reduction of green house gas emissions. In addition, the H_2/CO ratio obtained by CO_2 reforming of methane is more convenient for further applications [5–9]. A low H_2/CO ratio favors the methanol to gasoline process for ethane, propane and aromatics from methanol and oxo-synthesis to alcohols. Hydroformilation and acetic acid synthesis is also favored at low H_2/CO ratios [10].

During the last two decades, a great effort has been dedicated to the development of industrially suitable catalysts for methane reforming [4–9, 11]. Ni-based catalysts are the most widely used due to its lower cost and activity; however, they are less active compare to Ru, Rh and Ir and tent to deactivate by oxidation and carbon formation, which can occur via methane decomposition (Eq. 1) and Boudouard reaction (Eq. 2):

$$CH_4 \rightleftarrows 2H_2 + C_{(s)}\ \Delta H_{298} = 75\ \text{kJ/mol} \quad (1)$$

$$2CO \rightleftarrows CO_2 + C_{(s)}\ \Delta H_{298} = -173\ \text{kJ/mol} \quad (2)$$

New types of catalysts are currently developed to minimize the kinetics of carbon formation [11–14]. Among those solids, perovskites has been used since these mixed-oxides, when reduced; produce small particles in the order of nanometers with high dispersion inhibiting carbon formation [10–14]. Additionally, it has been reported [15] that niobium has the ability to trap Ni during the catalytic cracking on Ni/Nb_2O_5–SiO_2 which will also inhibit carbon formation. An increasing interest in the development of niobium based materials is shown due to its high activity in a series of reactions such as hydrogenation, dehydrogenation and oxidation [15]. Many rare-earth orthoniobates are isostructural with $BiVO_4$ and mineral fergusonite $YbNbO_4$. One of them is the lanthanum orthoniobate, $LaNbO_4$ with a scheelite-type structure. Scheelite structure has tetragonal symmetry and overall composition (ABO_4), with B cations beings tetrahedral coordinated to oxygen with links of equal length [16].

Another important property of niobium oxides is its facility to form solid solutions with other oxides. Niobium could be present in the solid both as a support and as superficial species (redox sites) [17]. In doping amounts, niobium oxide increases the activity and selectivity of various reactions and the stability and life of the catalyst.

In this work, perovskite-related mixed-oxides based on LaNiNb were synthesized by the auto combustion method and used as catalyst precursors in the dry reforming of methane to minimize carbon formation and enhance activity/selectivity to syngas production. The effect of substitution of La by Sr on the activity and stability of the catalysts was also studied. $LaNiO_3$ perovskite-type oxide and lanthanum orthoniobate $LaNbO_4$ a scheelite-type structure were used as reference solids.

2 Experimental

2.1 Mixed-Oxides Synthesis and Characterization

The mixed-oxide solids were synthesized by modification of the auto-combustion method [18]. A niobium solution prepared from $[NH_4(NbO)(C_2O_4)_2(H_2O)_2]2H_2O$ was added with continuous stirring to a solution of glycine, 99%, Sigma, together with solutions of the precursor salts of B and A cations: Ni $(NO_3)_3{\cdot}6H_2O$, 99%, Riedel-de Haën, $La(NO_3)_3{\cdot}6H_2O$, 99%, Merck and $Sr(NO_3)_2$, 99%, Riedel-de Haën, with molar ratio $NO_3^-/NH_2 = 1$ as describe elsewhere [19]. To obtain the Ruddlesden–Popper type perovskite the solids were calcined following the protocole described by Amow et al. [17]. Similarly, a solid was synthesized which after calcined at 500 °C under air atmosphere was impregnated with Ni (24%) by the incipient wetness method.

The synthesized solids were characterized by FT-IR, X-ray diffraction analysis (XRD), BET specific surface area, TGA-DTA analysis, TPR and transmission electron microscopy (TEM).

The structure of the as synthesized perovskites was determined by means of a Brucker Analytical X-Ray System using Cu Kα radiation with $\lambda = 1{,}5406$ Å for crystalline phase detection between 10° and 90° (2θ) and compare with JCPDS standard files software using the program database PCPDFWIN. The particle size diameter were calculated using (1 0 1) reflection and the Scherrer formula [20]. Surface areas were measured by a multiple-point BET procedure using nitrogen–argon adsorption at liquid nitrogen temperature with 30% N_2 in Ar in a Micromeritics Tristar 3300 system. The reducibility of these precursor mixed-oxides was studied by TPR analysis performed in a Thermo-Quest TPD/TPR 1100 system using 0.07 g of the sample with 10% H_2 in Ar stream (20 mL/min). The temperature was raised from room temperature to 1000 °C at a rate of 10 °C/min. The TGA-DTA analyses to determine the amount of carbon formed was performed by a TA Instrument model 2900 using air (10 mL/min).

2.2 Activity Tests

Activity tests were performed using 50 mg of catalyst diluted in 150 mg of sea sand in a 20-mm ID quartz reactor at atmospheric pressure operated in a fixed-bed continuous

flow system (CH_4:CO_2 = 1:1, Ar as diluents, Tr = 25–750 °C, WHSV = 24 L/h g). Before the catalytic tests, the solids were reduced in H_2 (25 mL/min, 700 °C, 6 h). After reduction, the system was swept with Ar for 1 h., and adjusted to the reaction temperature. The water produced during reaction, was condensed before passing the reactants and products to the analyzing system, which consisted of an on-line gas chromatograph (Perkin Elmer Auto System XL) equipped with an automatic injection, TCD and provided with a Carbosieve SII 80/100 (12′×1/8′ OD SS) column as previously described [20]. The CH_4 and CO_2 conversions were defined as the CH_4 and CO_2 converted per total amount of CH_4 and CO_2 fed, respectively. The selectivity to CO was calculated based in carbon balance and defined as S_{CO} (%) = $\eta_{CO}/[\eta_{CH_4(c)} + \eta_{CO_2(c)}] \times 100$; while hydrogen selectivity was calculated as S_{H_2} (%) = $[\eta_{H_2}/2\eta_{CH_4(c)}] \times 100$, where η_{CO} and η_{H_2} are the moles of CO and hydrogen produced and $\eta_{CH_4(c)}$ and $\eta_{CO_2(c)}$ are the amounts of methane and carbon dioxide converted, as described elsewhere [21]. Stability tests were performed at 700 °C for 24 h.

Carbon formation on the catalysts after reaction was determined by TGA-DTA analysis and compared to calculated values using the CO selectivity as reference, expressed as $NC/N_o = (1 - S_{CO})/(N_{CH_4(c)} + N\eta_{CO_2(c)})$, where NC and N_o represent the moles of carbon formed and the initial moles of methane and carbon dioxide respectively.

3 Results and Discussion

3.1 Characterization by FT-IR, BET, TEM and XRD Analyses

The $LaNi_{1-x}Nb_xO_3$ series showed two IR bands as seen in Table 1. The high frequency bands ν_1, between 654 and 576 cm^{-1} associated to the stretching vibration of the central atom of the NiO_6 and oxygen atoms placed in the upper and lower position of the octahedral. These bands are associated to the bond strength between the central atom and the oxygen atoms. The larger the value of this magnitude, the stronger the Ni–O bond and the stability of the precursor perovskite structure are. The low frequency band ν_2, at 523–420 cm^{-1} corresponds to the deformation frequency produced by the angle change between the central atom and the oxygen atoms at the corner of the octahedral. As seen on Table 1, most solids shown ν_1 ~650 cm^{-1} while the position for the reference precursor $LaNiO_3$ is at ν_2 ~576 cm^{-1}, indicating that the substitution of Ni by Nb to produce $LaNi_{1-x}Nb_xO_3$ series give rise to more thermodynamically stable structures.

Table 1 FT-IR bands frequencies of $LaNi_{1-x}Nb_xO_3$ and La_2NiO_4 series

Precursor	ν_1 (cm^{-1})	ν_2 (cm^{-1})
$LaNiO_3$	576	476
$LaNb_{0.1}Ni_{0.9}O_4$	648	440
La $Nb_{0.2}Ni_{0.8}O_4$	651	523
$LaNb_{0.3}Ni_{0.7}O_3$	654	ND
$LaNb_{0.4}Ni_{0.6}O_3$	602	ND
$LaNb_{0.5}Ni_{0.5}O_3$	654	422
La_2NiO_4	653	502

Table 2 shows BET specific surface areas, XRD analyses and particle size diameter results. It is observed that the extent of substitution (x) of Ni by Nb has a notable influence on the specific surface areas of $LaNi_{1-x}Nb_xO_3$ precursor series as compared to the reference solids $LaNiO_3$ and $LaNbO_4$, with the larger surface areas at x = 0.3–0.6 as can be observed on Fig. 1. As expected, the particle size decreases as the specific surface areas increase. Concerning the particle size distribution, it was observed that depending on the extent of substitution (x), particles in the range of 5–60 nm were obtained, as determined by TEM measurements (Fig. 2).

TEM micrographs of a series of precursors are shown in Fig. 3. For $LaNb_{0.3}Ni_{0.7}O_4$ (Fig. 3a) small cubic shaped particles are observed dispersed on a white matrix, with particles sizes in the interval of 37–90 nm. Increasing Nb content not only changes the particle size distribution to lower values but it also changes the well defined cubic shape of the grains to rounded shaped particles as seen by TEM analysis (Fig. 3b). For the impregnated solid Ni(25%)/$LaNbO_4$–$La_2O_2CO_3$, (Fig. 3c) a homogeneous particle size distribution with particles in the order of ~10 nm was obtained, the ring shaped XRD pattern indicating formation of a polycrystalline material. Addition of Sr promotes formation of larger cubic shaped particles of ~40 nm (Fig. 3d).

In agreement with TEM results, the XRD analysis (Table 2; Fig. 4) shows that the auto combustion method favors Ni crystallization as a perovskite-type structure while Nb forms a scheelite-type structure depending on Nb content. For low niobium content ($x \leq 0.3$) $LaNiO_3$ is formed, while for higher niobium content ($x \geq 0.7$) Ni formed part of a structure related to $LaNbO_4$ ortho niobate with scheelite-type structure [22]. It was observed that the auto combustion process became less intense as the niobium content increases, due to the fact that the niobium precursor salt does not contain nitrates, producing a non-equimolar NO_3^-/NH_2 ratio [18]. When solids are calcined at 500 °C in air; a mixture of oxides compose of La_3NbO_7 ($LaNbO_4 + La_2O_3$) and $La_2O_2CO_3$ was obtained (Table 2). This mixed-oxide was impregnated with Ni since it has been established that the

Table 2 BET specific surface areas, XRD analyses and particle size diameter of synthesized precursor solids

Precursor	T_{Calc} (°C)	S.A. (m^2g^{-1})	Dp (nm)	XRD phases
$LaNiO_3$	800	4	15	$LaNiO_3$
$LaNi_{0.9}Nb_{0.1}O_3$	800	8	13	$LaNiO_3$
$LaNi_{0.8}Nb_{0.2}O_3$	800	11	11	$LaNiO_3$, $LaNbO_4$
$LaNi_{0.7}Nb_{0.3}O_3$	800	17	8	$LaNiO_3$, $LaNbO_4$
$LaNi_{0.6}Nb_{0.4}O_3$	800	19	8	$LaNiO_3$, $LaNbO_4$
$LaNi_{0.5}Nb_{0.5}O_3$	800	19	11	$LaNiO_3$, $LaNbO_4$
$LaNi_{0.3}Nb_{0.7}O_4$	800	9	10	$LaNiO_3$, $LaNbO_4$
$LaNi_{0.2}Nb_{0.8}O_4$	800	8	7	La_2NiO_4, $LaNbO_4$
$Ni(24\%)/La_2O_3$	500	12	ND	$LaNiO_3$, La_2O_3
$Ni(24\%)/LaNbO_4–La_2O_2CO_3$	500	25	13	$LaNbO_4$, $La_2O_2CO_3$
$La_2NiO_{4.15}$	1100	5	30	La_2NiO_4, $LaNiO_3$, $LaNbO_4$, NiO
$La_2Ni_{0.8}Nb_{0.2}O_4$	1100	9	22	La_2NiO_4, $LaNiO_3$, $LaNbO_4$, NiO
$La_{0.8}Sr_{0.2}Ni_{0.8}Nb_{0.2}O_3$	800	13	38	$LaNiO_3$, $La_3Ni_2O_7$, $Sr_5LaNb_{10}O_{30}$, NiO

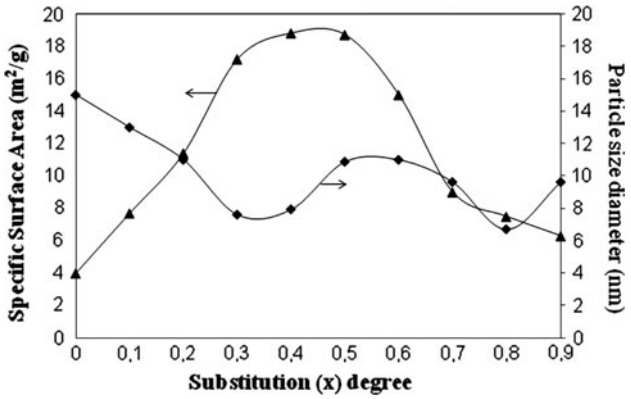

Fig. 1 Effect of the substitution degree (x) of Ni by Nb on the specific surface area and particle size distribution

presence of $La_2O_2CO_3$ favors CH_4 oxidation and La_2O_3 regeneration, inhibiting carbon formation during the dry reforming of methane [5, 15, 18].

Due to the similarity of La and Sr ionic radii, introduction of doping quantities of Sr to the $LaNi_{0.8}Nb_{02}O_3$ mixed-oxide system produces a mixture of oxides (Table 2), with Sr dissolved in the $LaNbO_4$ matrix, which produces oxygen vacancies in the system to compensate for charge deficiencies when Sr^{2+} substitute La^{3+}. Even that Nb could be present in different coordination states, it was found mainly in a tetrahedral coordination as NbO_4, inhibiting the partial substitution of Nb by Ni which is in an octahedral coordination (NiO_6) [23].

The XRD analyses of Ruddlesden-Popper structures La_2NiO_4 and $La_2Ni_{0.8}Nb_{0.2}O_4$ precursors after calcined are

Fig. 2 Particle size distribution as obtain by TEM analysis

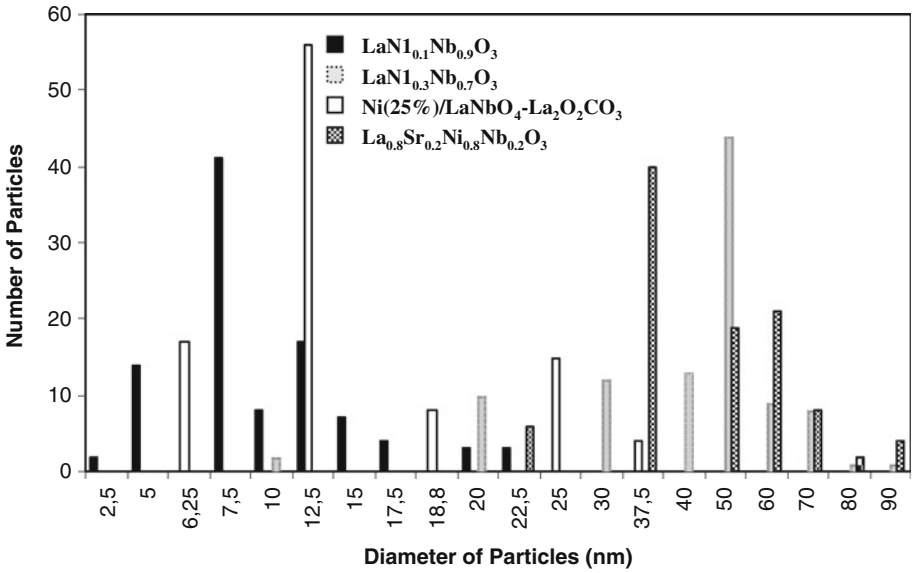

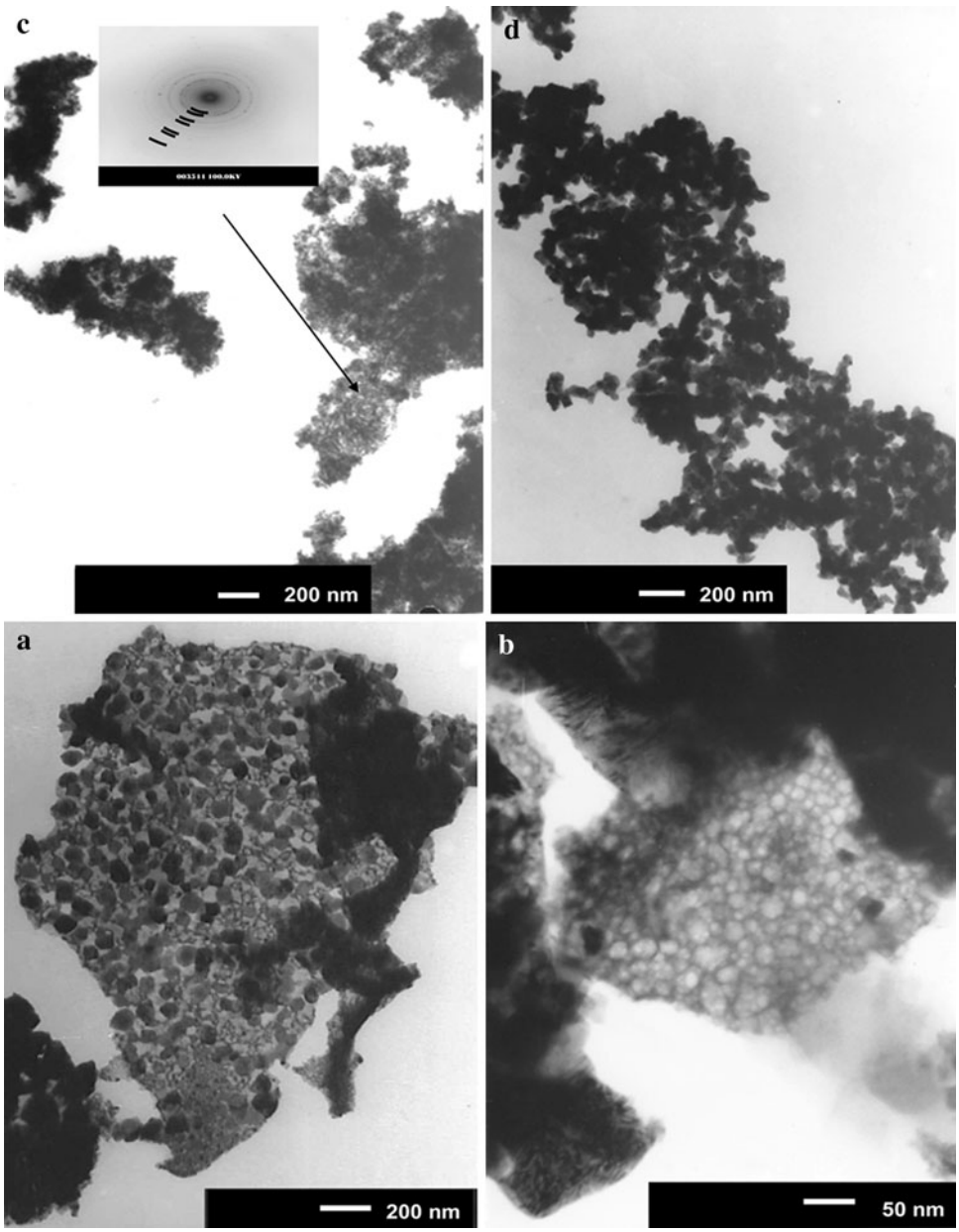

Fig. 3 TEM micrographs: (**a**) $LaNi_{0.3}Nb_{0.7}O_3$, (**b**) $LaNi_{0.1}Nb_{0.9}O_3$, (**c**) $Ni(25\%)/LaNbO_4$–$La_2O_2CO_3$, (**d**) $La_{0.8}Sr_{0.2}Ni_{0.8}Nb_{0.2}O_3$

shown in Fig. 5. It is observed that the only phase present is $La_2NiO_{4.15}$ (JCPDF 801910), which crystallizes in a tetragonal phase [17]. For La–Ni–Nb–O system a complex pattern was obtained showing the presence of La_2NiO_4, $LaNiO_3$, $LaNbO_4$ and NiO as main phases. These results demonstrate the presence of non-stequiometry solids with an oxygen excess in the precursor solid $La_2NiO_{4+\delta}$, as previously reported by Weng et al.[24] and Mogni et al. [25] who reported a $\delta = 0.18$ value.

The XRD profile of $LaNi_{0.9}Nb_{0.1}O_3$ precursor after reduction with H_2 is shown in Fig. 6. It is observed that the perovskite type structure disappear giving rise to $La(OH)_3$ (JCPDS 83-2034) and Ni^o (JCPDS 87-0712) the latter with a characteristic peak at 44.4° 2θ. The presence of Ni^0 is the result of the reduction reaction of the perovskite producing highly dispersed Ni^o particles on $La(OH)_3$. Due to the low amount of Nb in this solid, it presence was not detected by XRD.

3.2 TPR Studies

TPR analysis on the precursor mixed-oxide solids indicates reduction of Ni to Ni° as the only reduced phase, producing highly dispersed Ni particles supported on a mixture of oxides such as La_2O_3, $LaNbO_4$ and other irreducible NbO_x-oxides present in the precursors as seen by XRD and TEM analysis.

Several reduction peaks can be observed in all the TPR range consistent with a stepwise reduction process due to

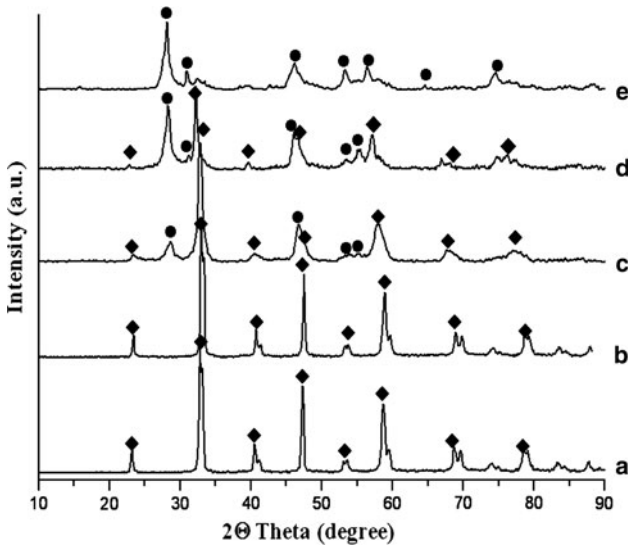

Fig. 4 X-ray diffraction profiles of synthesized perovskites: (*a*) $LaNiO_3$; (*b*) $LaNi_{0.9}Nb_{0.1}O_3$; (*c*) $LaNi_{0.5}Nb_{0.5}O_3$; (*d*) $LaNi_{0.3}Nb_{0.7}O_3$; (*e*) $LaNbO_4$; $LaNiO_3$ (*filled diagonal*); $LaNbO_4$ (*filled circle*)

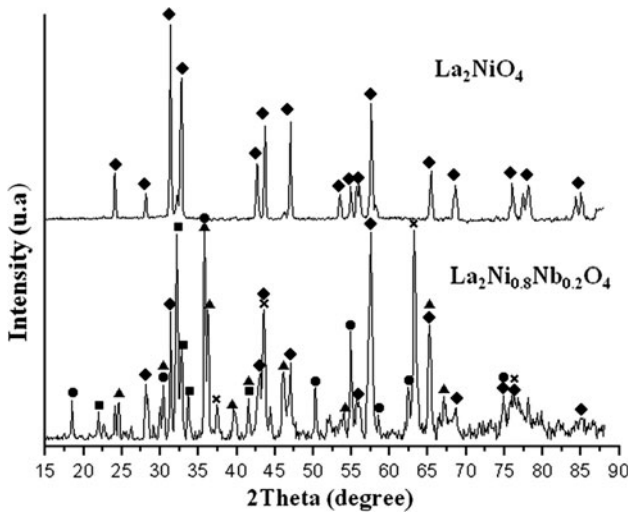

Fig. 5 X-ray diffraction profiles of calcined Ruddlesden-Popper Perovskites La_2NiO_4 and $La_2Ni_{0.8}Nb_{0.2}O_4$: (*filled diagonal*) La_2NiO_4, (*filled triangle*) $LaNbO_3$, (*cross*) NiO (*filled square*) $LaNiO_3$, (*filled circle*) NbO

the presence of different Ni species with different particle size and to formation of oxygen deficient intermediates. At low Ni content where smaller particle sizes are expected, the reduction temperature increases as seen on Fig. 7, where the reduction profiles of $LaNi_{1-x}Nb_xO_3$ perovskite type oxide and the reference precursors are shown. Three peaks are observed. The interval between 300-400 °C, corresponds to the formation of $La_4Ni_3O_{10}$, resulting from the reduction of Ni^{3+} as shown by (Eq. 4). A second peak between 400 and 500 °C corresponding to the reduction to Ni^{2+} trough formation of La_2NiO_4, (Eq. 5) and the third peak at 580–700 °C indicates the reduction of Ni^{2+} to Ni^0

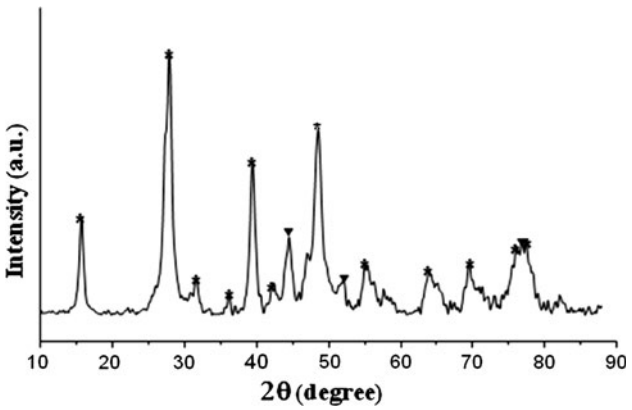

Fig. 6 X-ray diffraction profiles of reduced $LaNi_{0.9}Nb_{0.1}O_3$: (*asterisk*) La_2O_3, (*filled inverted triangle*) Ni^0

according to (Eq. 6), in agreement with our previously reported results using in situ TPR-XRD analysis [6].

$$4LaNiO_3 + 2H_2 \rightarrow La_4Ni_3O_{10} + Ni^{\circ} + 2H_2O\left(300 - 400^{\circ}C\right) \quad (4)$$

$$La_4Ni_3O_{10} + 3H_2 \rightarrow La_2NiO_4 + 2Ni^{\circ} + La_2O_3 + 3H_2O\left(400 - 500^{\circ}C\right) \quad (5)$$

$$La_2NiO_4 + H_2 \rightarrow Ni^{\circ} + La_2O_3 + H_2O\left(500 - 700^{\circ}C\right) \quad (6)$$

Ruddlesden–Popper perovskite reduction profiles (not shown) are similar to the previously described behavior for the other solids. However, higher reduction temperatures (790–850 °C) are needed since as shown by FT-IR analysis they are thermodynamically more stable.

3.3 Activity Tests

Catalytic tests showed that, depending on the Nb content, the perovskite-related LaNiNb mixed-oxides precursors previously reduced at 700° C are highly active in the dry reforming of methane (Table 3). Catalytic activity increases for Nb contents in the order of $x \geq 0.3$, with $LaNi_{0.5}Nb_{0.5}O_3$ being the most active precursor producing CH_4 and CO_2 conversions 96 and 78% respectively, remaining constant for ~30 h (Fig. 8).

The high activity and stability shown by this precursor is due to formation small nanoparticles (~11 nm) of Ni^0 highly dispersed on the surface of the oxides (Fig. 9a) and to the presence of $La_2O_2CO_3$ which allows methane reforming and the formation of La_2O_3 [5, 9, 13, 19]. The initial $La_2O_2CO_3$ phase is generated by adsorption of CO_2 on La_2O_3, inhibiting carbon formation. The high activity shown by this solid compare to that of Ni (25%)/La_2O_3 assessed the importance of the presence of niobium on these catalysts.

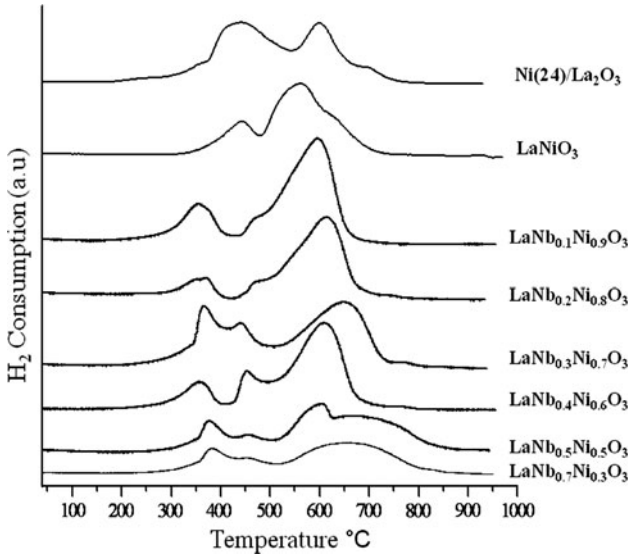

Fig. 7 TPR analysis of the precursor mixed-oxide solids

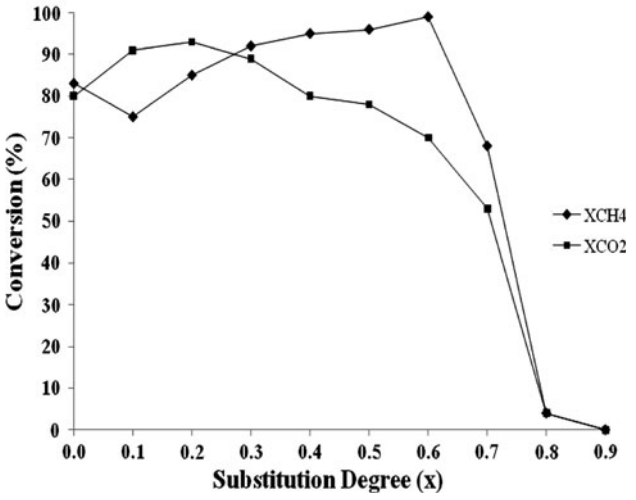

Fig. 8 Effect of the substitution degree of Ni by Nb in the catalysts activity

The presence of Nb increases the activity of the solids compare to that observed when $LaNiO_3$ is used as precursor. The H_2/CO selectivity ratio close to 1 for the precursors with $x \geq 0.5$ during the dry reforming of methane corroborates the absence of secondary reaction on those solids (Table 3). This behavior could be attributed to the presence of lamellar structures of the perovskite related mixed-oxides which after reduction, produce highly dispersed Ni^0 particles strongly interacting with Nb acidic species such as NbO_4 and Nb_2O_3. Even though this type of interaction is not clearly establish, Xiancai et al. [26] reported that Lewis acidity of the support has an important effect on the metallic phase favoring its residence on those sites and inhibiting sintering of the metallic particles to form large clusters.

Long run tests performed on $LaNi_{0.7}Nb_{0.3}O_3$ precursor catalyst showed conversions near the thermodynamic equilibrium which remain constant for 120 h and equal to 92 and 89% for CH_4 and CO_2 respectively, assessing the stability of the synthesized catalysts. Similarly, Ni (25%)/$LaNbO_4 - La_2O_2CO_3$ showed high activity for the dry reforming reaction with CH_4 and CO_2 conversion of 80 and 94% respectively.

The Sr doped solid showed high methane (94%) and CO_2 (80%) conversions due to the fact that partial substitution of La by Sr produces oxygen vacancies in the niobium tetrahedral coordination sphere of $La^{3+}_{1-x}Sr^{2+}_{x}Nb^{5+}O^{2-}_{4-x/2}$ increasing CO_2 adsorption to form $SrCO_3$ which inhibit carbon deposits.

The amount of carbon formed in these solids was also dependent on Nb content being 2.6% for $x = 0.5$ as determined by TGA-DTA analysis. No deactivation of the solids was observed due to the fact that carbon was formed as nanotubes which could re-disperse the Ni particles, as

Table 3 Dry reforming of methane

Precursor solid	X_{CH4} (%)	X_{CO2} (%)	$\eta H_2/X_{CH_4(conv)}$	$\eta H_2/\eta CO$
$LaNiO_3$	83	89	1.47	0.83
$LaNi_{0.9}Nb_{0.1}O_3$	75	89	2.05	0.96
$LaNi_{0.8}Nb_{0.2}O_3$	85	83	2.15	1.03
$LaNi_{0.7}Nb_{0.3}O_3$	92	85	2.03	0.95
$LaNi_{0.6}Nb_{0.4}O_3$	95	85	1.63	0.86
$LaNi_{0.5}Nb_{0.5}O_3$	96	78	1.63	0.86
$LaNi_{0.4}Nb_{0.6}O_4$	86	77	0.85	0.76
$LaNi_{0.3}Nb_{0.7}O_4$	68	56	0.71	0.60
La_2NiO_4	66	69	0.97	0.71
$La_2Ni_{0.8}Nb_{0.2}O_4$	91	94	1.50	1.00
$La_{0.8}Sr_{0.2}Ni_{0.8}Nb_{0.2}O_3$	94	80	1.62	0.85
Ni(25%)/$LaNbO_4$-$La_2O_2CO_3$	80	94	1.50	0.99
Ni(24%)/La_2O_3	43	67	1.55	0.70

tr = ~30 h, WHSV = 24 L/h g, $CH_4/CO_2 = 1$, Tr = 700 °C, Tred = 700 °C—5 h

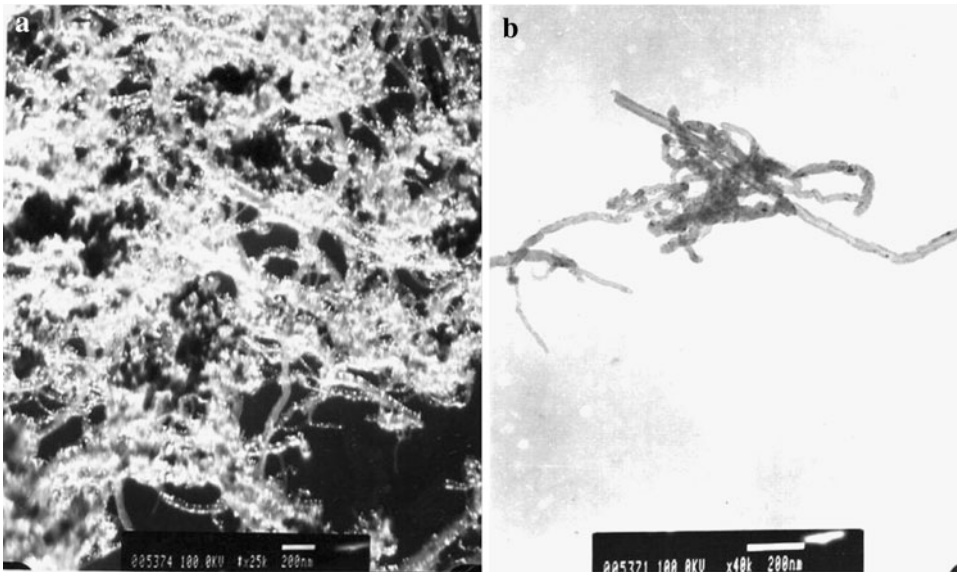

Fig. 9 TEM Micrographs of $LaNi_{0.5}Nb_{0.5}O_3$ after reaction: (**a**) dark field image, (**b**) clear field imag

evidence on Fig. 9 for the solid with $x = 0.5$. The size of the nanotube is given by the presence of Ni in the entry of the pore which corresponds to 30-40 nm. The transparency of the nanotube is indicative of multi-walled nanotube formation.

4 Conclusions

It was observed that the synthesis method highly influence the solid structure of perovskite-related LaNiNb mixed-oxides which depends on niobium content, giving rise to the polycrystalline lanthanum orthoniobate, $LaNbO_4$ scheelite type structure, alternating with La_2O_3 and/or Nb_2O_5 layers and lamellar structures of Ruddlesden–Popper type (LaO) $LaNiO_3$.

Niobium could be present in the solid both as a support and as superficial species (redox sites). When small amounts are added to the catalyst it remarkably enhance catalytic activity and prolong catalyst life

Reduction of the precursor solids produce a series of catalysts where metallic Ni appears highly crystalline and homogeneously dispersed on the oxide matrix formed by La_2O_3 and the unreduced Nb phases with a high metallic dispersion which favors the activity and stability of the catalyst inhibiting carbon formation during the reforming reaction.

Introduction of doping quantities of Sr into $LaNi_{0.8}Nb_{0.2}O_3$ structure produced a mix of oxides with Sr dissolved in the lanthanum orthoniobate structure $LaNbO_4$ due to the similarity of ionic radii of La and Sr.

Ruddlesden-Popper type perovskite oxides are good catalytic precursors for the reforming of methane: under the reaction conditions conversions near the thermodynamic equilibrium were attained which remains for long periods of time assessing the stability of the synthesized catalysts.

Acknowledgements The authors thank Brazilian Metallurgy and Mineral Company CBMM, Araxá, MG-Brazil, for the Niobium samples supplied and the Council of Scientific and Humanistic Development of Venezuelan Central University (UCV-CDCH) and the Draft Law on Science and Technology (LOCTI), through projects PG-03-00-6504-2006 and LOCTI-2008-2009 respectively, for financial support.

References

1. Somorjai GA, McCrea K (2001) Appl Catal A Gen 222:3–18
2. Lira E, Lopez CM, Oropeza F, Bartolini M, Alvarez J, Goldwasser MR, Lopez Linares F, Lamonier Jean-François, Josefina Perez Zurita M (2008) J Mol Catal A Chem 281:146–153
3. Nagaoka K, Jentys A, Lercher JA (2005) J Catal 229:185–196
4. Basini L (2005) Catal Today 106:34–40
5. Rivas ME, Fierro JLG, Guil-López R, Peña MA, La Parola V, Goldwasser MR (2008) Catal Today 133–135:367–373
6. Rivas ME, Fierro JLG, Goldwasser MR, Pietri E, Perez Zurita MJ, Griboval-Constant A, Leclercq G (2008) Appl Catal A Gen 344:10–19
7. Hori C, Rivas ME, Fierro JLG, Goldwasser MR, Griboval A (2008) J Power Source 184:265–275
8. Erdohelyi A, Fodor K, Szailer T (2004) Appl Catal B Environ 53:153–160
9. Goldwasser MR, Rivas ME, Pietri E, Pérez Zurita MJ, Cubeiro ML, Griboval-Constant A, Leclercq G (2005) J Mol Catal A Chem 228:325–331
10. Goldwasser MR, Dorantes V, Pérez-Zurita MJ, Sojo PR, Cubeiro ML, Pietri E, González-Jiménez F, Lee Ng, Moronta D (2003) J Mol Catal A Chem 193:227–236
11. Martinez R, Romero E, Guimon C, Bilbao R (2004) Appl Catal A Gen 274:139–149
12. Batiot-Dupeyrat C, Valderrama G, Meneses A, Martínez F, Barrault J, Tatibouët JM (2003) Appl Catal A Gen 248:143–151
13. Goldwasser MR, Rivas ME, Pietri E, Pérez Zurita MJ, Cubeiro ML, Griboval-Constant A, Leclercq L, Leclercq G (2003) Appl Catal A Gen 225:45–57

14. Pereira MM, Pereira EB, Lam YL, dos Santos T, Schmal M (2000) Stud Surf Sci Catal 130:2339–2344
15. Tanabe K (2003) Catal Today 78:65–77
16. Parlinski K, Hashi Y, Tsunekawa S, Kawazoe Y (1997) J Mater Res 12(9):2428–2437
17. Amow G, Davidson IJ, Skinner SJ (2006) Solid State Ionics 177:1205–1210
18. Valderrama G, Goldwasser MR, de Navarro C Urbina, Tatibouët JM, Barrault J, Batiot-Dupeyrat C, Martinez F (2005) Catal Today 107–108:785–791
19. Valderrama G, Kiennemann A, Goldwasser MR (2010) J Power Sources 195:1765–1771
20. Goldwasser MR, Rivas ME, Lugo ML, Pietri E, Pérez-Zurita J, Cubeiro ML, Griboval-Constant A, Leclercq G (2005) Catal Today 107–108:106–113
21. Rivas I, Álvarez J, Pietri E, Pérez Zurita MJ, Goldwasser MR (2010) Catal Today 149(3–4):388–393
22. Sleight AW (1977) In: Burton JJ, Garten RL (eds) Advanced materials in catalysis. Academic Press, San Diego, p 181
23. Maschio S, Bachiorrini A, Di Monte R, Montanaro L (1995) J Mater Sci 30:5433–5437
24. Weng X, Boldrin P, Abrahams I, Skinner SJ, Kellici S, Wenga Xiaole, Darr JA (2008) J Solid State Chem 181:1123–2123
25. Mogni L, Prado F, Ascolani H, Abbate M, Moreno M, Manthiram A, Caneiro A (2005) J Solid State Chem 178:1559–1568
26. Xiancai Li, Min Wu, Zhihua Lai, Fei He (2005) Appl Catal A Gen 290:81–86